2 Physical Basis and Principles of Action of Microbubble-based Contrast Agents

Emilio Quaia

CONTENTS

2.1 Introduction

Microbubble-based contrast agents consist of microbubbles of air or other gases, encapsulated by a shell of different composition and with a diameter of approximately 2–6 μm. The high difference in acoustic impedance between the gas in the microbubble and the surrounding tissue in vivo makes microbubbles highly reflective resulting in the enhanced acoustic backscattering from blood by up to 27 dB in both colour and spectral Doppler modes (Forsberg et al. 1999).

The oscillation of the microbubble under US beam is governed by parameters such as resonance frequency, pulse repetition frequency, acoustic power, the filling gas, damping coefficients and shell properties. Besides the other factors, the local acoustic power is the principal parameter affecting microbubbles behaviour (Powers et al. 1997; Correas et al. 2001). At low acoustic power, the microbubbles destruction from the US beam is minimized and microbubbles oscillate synchronously with the incident US and emit non-linear echoes. With increasing acoustic power of the insonating US beam, signals returning from microbubbles are increased by several orders of magnitude due to interactions between the insonating beam and the microbubbles, which include fundamental scattering, harmonic resonance and microbubble destruction.

E. Quaia, MD
Assistant Professor of Radiology, Department of Radiology, Cattinara Hospital, University of Trieste, Strada di Fiume 447, 34149 Trieste, Italy

2.2 Microbubble Persistence in the Bloodstream

To act as effective contrast agents in the peripheral circulation, microbubbles have to persist in the bloodstream. Various chemical strategies have been adopted to produce stabilized gas microbubbles in the peripheral circulation and the different compositions have an important influence upon the performance of the resulting agent.

2.2.1 Diffusibility of the Filling Gas

The first factor which determines the persistence of microbubbles in the peripheral circle is the diffusibility of the filling gas throughout the peripheral shell. The diffusibility, expressed by the diffusion coefficient, and the solubility of the filling gas in the blood, strongly affect microbubble persistence in the circle, according to the following equation:

$$T = \frac{\rho R^2}{2 D C_s} \quad (1)$$

where T = microbubble persistence in the blood, ρ = density of the gas, R = initial radius of the microbubble, D = diffusion coefficient of the gas in the

substance of the shell, C_s = saturation coefficient of exchange of gas between aqueous and gaseous phases, which is higher in gas with increased solubility in the blood.

2.2.2 Surface Tension

Equation 1 is an effective approximation of microbubble persistence in the bloodstream. However, surface tension is another important mechanism responsible for the disappearance of the filling microbubble gas in a gas saturated liquid. The microbubble shell contains surface-active molecules, namely phospholipids, which act as a surfactant reducing the surface tension. The surfactant layer exerts a counterpressure against the tendency of surface tension and other forces to cause gas diffusion from a microbubble. The relation of the surface tension with microbubble dissolution was shown by Frinking (1999):

$$\frac{dR}{dt} = D \times L \left(\frac{\frac{C_i}{C_s} - 1 - \frac{2S_T}{Rp_0}}{1 + \frac{4S_T}{3Rp_0}} \right) \left(\frac{1}{R} + \frac{1}{\sqrt{\pi Dt}} \right) \quad (2)$$

where $\left(\frac{dR}{dt}\right)$ = variation of microbubble radius (R), with time (t) which is related to microbubble disappearance from the peripheral circle; D = diffusion coefficient of the gas; L = Ostwald coefficient which corresponds to the ratio of the amount of gas dissolved in the surrounding liquid and in the gas phase per unit volume; C_i/C_s = ratio of the dissolved gas concentration to the saturation concentration; S_T = surface tension; p_0 = ambient pressure. In Eq. 2 the surface tension is shown to strongly affect the dissolution of microbubbles and the higher the surface tension, the lower the microbubble persistence.

2.2.3 Osmotic Pressure of the Filling Gas

Kabalnov et al. (1998) showed that the stability of a microbubble in the peripheral circle is related to the osmotic pressure of the filling gas which counters the sum of the surface tension and blood arterial pressure:

$$(C_G + C_A)K \times T = \frac{2S_T}{R} + p_b + p_{atm} \quad (3)$$

where C_G and C_A = concentration of the filling gas ($_G$) and air ($_A$), K = gas constant, T = absolute temperature, S_T = surface tension, R = bubbles radius, p_b = systemic blood pressure, p_{atm} = atmospheric pressure (101 kPa). The limited solubility in blood determines an elevated vapour concentration in the microbubble relative to the surrounding blood and establishes an osmotic gradient that oppose the gas diffusion out of the microbubble. After the initial size adjustment due to the effect of body temperature, the microbubbles will either swell or shrink depending on the partial pressure of the air in the bubble, followed by a period of slow diffusion of gas into the bloodstream (Forsberg and Tao Shi 2001).

2.2.4 Diffusion and Ostwald Coefficients

Diffusion and Ostwald coefficients also strongly determine the rate of decrease of the bubble radius, which is a direct measure for the disappearance rate of the microbubble:

$$-\frac{d}{dt}\left(C_G R^3\right) = 3RD_G L_G C_G \quad (4)$$

$$-\frac{d}{dt}\left(C_A R^3\right) = 3RD_A L_A \left(C_A - \frac{p_{atm}}{KT}\right) \quad (5)$$

where C_G and C_A = concentration of the filling gas ($_G$) and air ($_A$), R = bubbles radius, D_G, D_a and L_G, L_a = diffusion and Ostwald coefficients respectively for the filling gas ($_G$) and the air ($_A$), p_{atm} = atmospheric pressure (101 kPa), K = gas constant and T = absolute temperature. From Eqs. 4 and 5 it can be derived that the diffusion and Ostwald coefficients determine the rate of decrease of the bubble radius, which is a direct measure for the disappearance rate of the microbubble. Thus, microbubbles filled with gases having lower diffusion and/or the Ostwald coefficient will persist longer in the bloodstream (Fig. 2.1) (Correas et al. 1997). This result was reached with the introduction of new generation of microbubble-based agents.

2.2.5 Nature of the Peripheral Capsule

The nature of the encapsulating shell is the last fundamental factor which affects microbubble persistence in the bloodstream. Of course, the more

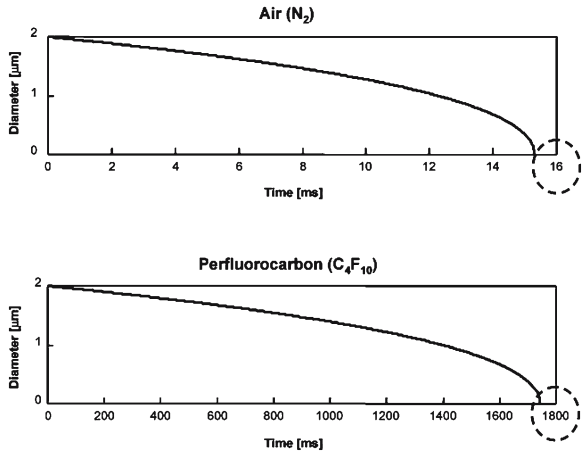

Fig. 2.1a,b. Difference of microbubble persistence in the bloodstream according to the filling gas: air (**a**) or perfluorocarbon gas (**b**), respectively. The microbubbles are completely dissolved when the diameter is equal to 0 and this happens after 16 ms for air (**a**) and 1800 ms for perfluorocarbon gas (**b**). (Images courtesy of Peter JA Frinking, Bracco Research, Geneva, Switzerland)

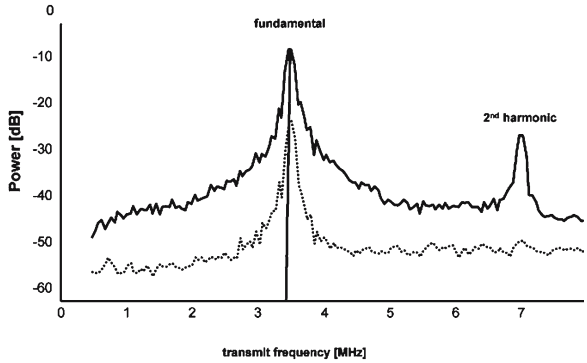

Fig. 2.2. Power spectral density of SonoVue for low (*broken line*) and high (*solid line*) acoustic power. The power of the backscattered signal presents a peak at the fundamental (resonant) frequency. (Image courtesy of Peter JA Frinking, Bracco Research, Geneva, Switzerland)

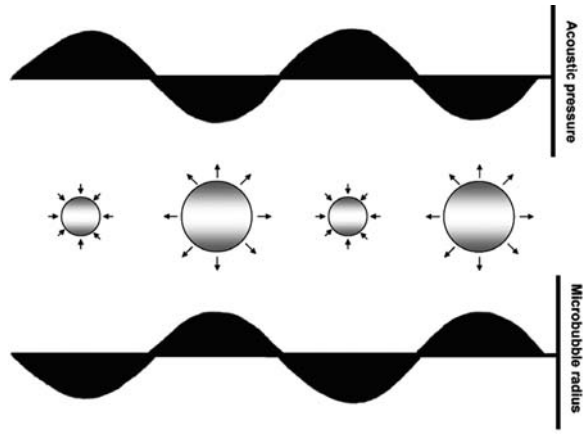

Fig. 2.3. Microbubble shows linear behaviour at very low acoustic power insonation. Microbubble radius presents a degree of compression at positive acoustic pressure which is equal to the degree of expansion at negative acoustic pressure.

stable the peripheral shell or the lower its solubility in water, the longer the microbubble persistence and echo-enhancing effect. Galactose-covered microbubbles present a low persistence for the high solubility of the sugar in the water. New generation microbubble-based agents present an albumin or phospholipids shell which present low solubility in water, further improving microbubble persistence in the bloodstream and the effect of scattering.

2.3 Physical Basis and Principles of Action

2.3.1 Resonant Frequency

The first theoretical description of free microbubble response to pressure was developed by Rayleigh (1917). Encapsulation of microbubbles affects their ability to oscillate, due to the presence of viscoelastic damping effects determined by the shell which influences the microbubble acoustic properties (de Jong et al. 1992, 1994; de Jong and Hoff 1994; Frinking and de Jong 1999). To produce effective backscattering microbubbles have to be insonated by their characteristic resonant frequency (Fig. 2.2) and the exposure to US at their resonant frequency forces microbubbles to contract and expand their diameter several-fold. At low acoustic power microbubbles produce a US signal with the same frequency as the sound that excited them (Fig. 2.3). By increasing the acoustic power of insonation microbubbles exhibit non-linear vibrations (Fig. 2.4) at their resonant frequency (f_0) generating signals at f_0, harmonics ($2f_0$, $3f_0$, $4f_0$, etc.) and subharmonics ($f_0/2$, $f_0/3$, etc.) (Fig. 2.5) (Forsberg et al. 1996; Shankar et al. 1998). At further higher acoustic power the expansion eventually disrupts the microbubbles shell generating a wide-band harmonic signal similar to a burst.

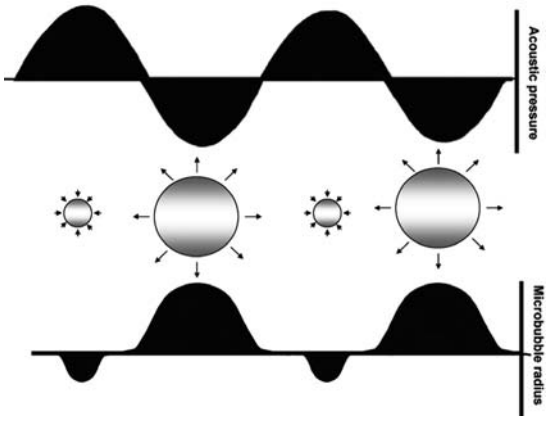

Fig. 2.4. Microbubble shows nonlinear behaviour if the acoustic power of insonation is progressively increased at the resonant frequency. With non-linear oscillation, the duration and degree of microbubble expansion is greater than its compression phase. This non-linear response to the insonation determines the production of harmonic frequencies.

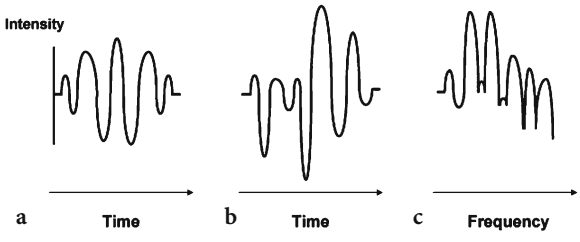

Fig. 2.5a–c. Microbubble non-linear behaviour. The transmitted acoustic wave (**a**) presents a definite periodic shape. The echo produced by microbubble resonance (**b**) presents an irregular shape in the time domain which becomes more definite in the frequency time (**c**) after Fourier transformation revealing multiple harmonic and subharmonic frequency components.

According to Anderson and Hampton (1980) the resonant – fundamental – frequency (f_0) is inversely related to the microbubble diameter and it may be expressed as:

$$f_0 \approx \frac{1}{2\pi R}\sqrt{\frac{3\gamma p_0}{\rho_0}} \qquad (6)$$

where R = microbubble diameter; γ = the ideal adiabatic constant of gas; p_o = ambient fluid pressure; ρ_0 = density of the surrounding medium. To derive Eq. 6 the damping caused by the surrounding medium is assumed negligible, as there are no effects due to bubble surface tension or thermal conductivity.

Considering the same model employed for the backscattering of an air-filled microbubble surrounded by a thin elastic shell, and taking into account the increased restoring force due to shell elasticity, a further equation was developed by de Jong et al. (1992):

$$f_0 \approx \frac{1}{2\pi r}\sqrt{\frac{3\gamma}{\rho}\left(P_0 + \frac{\pi}{3\gamma}\frac{S_e}{r}\right)} \qquad (7)$$

where S_e is the shell elasticity parameter which is defined as:

$$S_e = 8\pi\frac{R_0 - R_i}{1-\nu}E \qquad (8)$$

where R_i and R_o = inner (i) and the outer (o) diameter of the microbubble (the difference $R_o - R_i$ is the thickness of the shell), ν is the Poisson's ratio which describes the ratio of transverse contraction strain to longitudinal extension strain in the direction of stretching acoustic pressure (tensile deformation is considered positive and compressive deformation is considered negative) and E is the modulus of Young – modulus of elasticity in tension – which describes the stiffness of a microbubble.

2.3.1.1 Practical Application

According to Eq. 7 the higher the shell elasticity due to encapsulation, the higher the resonant frequency, at equivalent microbubble radius. Moreover, the lower the shell elasticity due to encapsulation, the lower the generation of harmonics, due to the damping provided by the shell viscosity which produces a notable decrease in the pulsation amplitude. So, for a stiff and thick shell the stability in the peripheral blood is higher if compared with a flexible and thin shell, but production of harmonics is lower. In practical terms, for any given US power and frequency, less acoustic signal can be expected from microbubbles with thick, stiff shells. Since microbubbles with thick and stiff shells present an increased resistance to the US acoustic power of insonation, the produced acoustical backscattering signal may be improved simply by increasing the acoustic power of insonation.

Moreover, according to Eq. 7, the ideal resonant frequency for a microbubble is inversely related to the square of its radius (de Jong et al. 1996; Frinking and de Jong 1999). The larger the microbubble radius, the lower the resonant frequency (Fig. 2.6), and the resonant frequency of a microbubble with a diameter of a few micrometres is comprised in the low MHz frequency range, which is employed

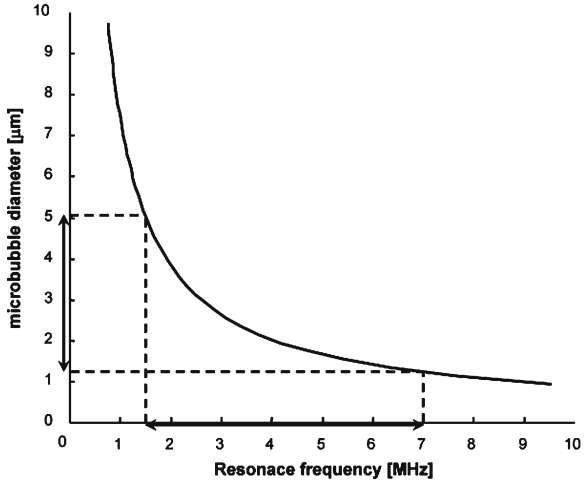

Fig. 2.6. Free air microbubble. Inverse hyperbolic relation between the resonance frequency and the microbubble diameter. (Image courtesy of Peter JA Frinking, Bracco Research, Geneva, Switzerland)

in abdominal US. Specifically, the resonant frequency for phospholipid-coated microbubbles with a diameters of 1–5 µm is approximately 4–0.6 MHz (Dayton and Ferrara 2002).

2.3.2 The Fundamental Equation of Microbubble Backscattering: Rayleigh–Plesset

The Rayleigh, Plesset, Noltingk, Neppiras, Poritsky equation, also known as the RPNNP equation and which was further developed by Church (1995), considers a free microbubble gas-filled model and describes both the linear and the non-linear characteristics of a shell-encapsulated microbubble.

In this model, the microbubble is considered coated by a continuous layer of incompressible solid elastic material, with a spherically symmetric motion, and surrounded by an incompressible liquid which presents infinite extent and a constant viscosity according to Newton's law. A Newtonian fluid is a fluid in which the shear stress – the ratio of force up to the area subjected to the force – is proportional to viscosity and velocity gradient (Chatterjee and Sarkar 2003). The rheological parameters (surface tension and viscosity) for microbubble-based agents may be calculated. The wavelength of the US field is assumed to be much larger than the microbubble diameter, and only the motion of the bubble surface is of interest. It is assumed that the vapour pressure remains constant during the compression and expansion phase, and that there is no rectified diffusion during the short period of exposure to US. The gas in the bubble is assumed to be ideal and compressed and expanded according to the ideal gas law with the polytropic exponent (Γ) remaining constant during vibration (Frinking 1999).

2.3.2.1 Motion of the microbubble wall

The first parameter to be considered in the backscattering is the motion of the microbubble wall (Frinking 1999):

$$\rho R R^{\bullet\bullet} + \frac{3}{2}\rho R^{\bullet 2} = p_L - p_0 \rho R^{\bullet 2} = p_L - p_\infty \qquad (9)$$

where ρ = density of the surrounding liquid medium (= 998 kg/m³); R = instantaneous microbubble radius; $R^{\cdot}$ = first time derivative of the radius (the velocity of the microbubble wall); $R^{\cdot\cdot}$ = second time derivative of the radius (the acceleration of the microbubble wall); p_L = liquid pressure at the microbubble wall; p_∞ = liquid pressure at infinity.

The assumption is that presence of the microbubble shell completely dominates the motion of the microbubble wall. Therefore, the microbubbles are considered to be elastic particles, which have an effective bulk modulus, K_{eff}, describing the elasticity of the shell, and a friction parameter describing the viscosity of the shell.

2.3.2.2 Bulk Modulus ≈ Elasticity of the Shell

The effective bulk modulus describes the elasticity of the shell. For a spherical volume V deformed by a quasi-static pressure change, ΔP determines the volume change of the microbubble and it is uniform over the microbubble surface. The volume strain (deformation) corresponds to –ΔV/V, where V is the initial volume and ΔV is the change in volume, while the volume stress (ΔP) corresponds to the ratio of the magnitude of the normal force to the area. The effective bulk modulus, K_{eff} (Frinking and de Jong 1999), is given by the ratio of the volume stress to the volume strain:

$$K_{eff} = -V\frac{\Delta P}{\Delta V} \qquad (10)$$

Since the volume is spherical, symmetric and defined by the radius, the volume strain can be written as:

$$\frac{\Delta V}{V} = \left(\frac{R}{R_0}\right)^3 - 1 \tag{11}$$

where R_0 is the initial microbubble radius. Combining Eqs. 10 and 11 gives:

$$\Delta P = -K_{eff}\left[\left(\frac{R}{R_0}\right)^3 - 1\right] \tag{12}$$

2.3.2.3 Friction Damping ≈ Viscosity of the Shell

The friction damping parameter describes the viscosity of the shell. Since the pressure change ΔP, determining the volume change of the microbubble, can be split into three parts: (1) the liquid pressure at the bubble wall (p_L); (2) the damping pressure caused by friction damping of the system bubble – liquid (p_d), and (3) the hydrostatic pressure (p_0), it may be expressed as:

$$\Delta P = p_L + p_d - p_0 \tag{13}$$

Substitution of Eqs. 12 and 13 into Eq. 9, and using the expanded expression for p_∞ ($p_\infty = p_0 + P_{(t)}$; where p_0 = hydrostatic pressure; $P_{(t)}$ = time-varying applied acoustic pressure) yields:

$$\rho R R^{\bullet\bullet} + \frac{3}{2}\rho R^{\bullet 2} = -K_{eff}\left[\left(\frac{R}{R_0}\right)^3 - 1\right] - p_d - P_{(t)} \tag{14}$$

By equating the damping pressure, multiplied by the bubble surface, to the damping force, an expression for p_d can be derived from the equation of motion of a damped forced oscillator:

$$4\pi R^2 p_d = \beta R^{\bullet} \tag{15}$$

where β is the mechanical resistance, R = instantaneous microbubble radius; $R^{\cdot}$ = first time derivative of the radius (the velocity of the microbubble wall).

According to the expression of Medwin (1977) for the total viscous and friction damping coefficient, $\delta_{tot} = \beta/\omega m$, where ω = insonating frequency of the applied acoustic field and m = effective microbubble mass [$(3/4)\pi R^3\rho$], the damping pressure can be written as:

$$p_d = \delta_{tot}\rho\omega R R^{\bullet} \tag{16}$$

where $\delta_{tot} = \delta_{rad} + \delta_{vis} + \delta_{th} + \delta_{fr}$, and δ_{rad} = damping coefficient due to reradiation; δ_{vis} = damping coefficient due to the viscosity of the surrounding medium; δ_{th} = damping coefficient due to heat conduction (Medwin 1977) and δ_{fr} = damping due to internal friction or viscosity of the shell (Hoff 1996).

Including friction damping, the final expression for the Rayleigh–Plesset theory is:

$$\rho R R^{\bullet\bullet} + \frac{3}{2}\rho R^{\bullet 2} = p_{go}\left(\frac{R_0}{R}\right)^{3\Gamma} + p_v - p_0 - \frac{2S_T}{R} - \delta_{tot}\omega\rho R R^{\bullet} - P_{(t)} \tag{17}$$

or

$$\rho R R^{\bullet\bullet} + \frac{3}{2}\rho R^{\bullet 2} = -K_{eff}\left[\left(\frac{R_0}{R}\right)^3 - 1\right] - \delta_{tot}\rho\omega R R^{\bullet} - P_{(t)} \tag{18}$$

or

$$\rho R R^{\bullet\bullet} + \frac{3}{2}\rho R^{\bullet 2} = p_{go} - p_0 - \frac{2S_T}{R} - \frac{4\eta}{R}R^{\bullet} \tag{19}$$

or

$$\rho R R^{\bullet\bullet} + \frac{3}{2}\rho R^{\bullet 2} = p_{go}\left(\frac{R_0}{R}\right)^{3\Gamma} - \frac{2S_T}{R} - \frac{4\eta R^{\bullet}}{R} - p_0 + P_{(t)}\sin\omega t \tag{20}$$

where R = instantaneous microbubble radius; $R^{\cdot}$ = first time derivative of the radius (the velocity of the microbubble wall); $R^{\cdot\cdot}$ = second time derivative of the radius (the acceleration of the microbubble wall); p_{go} = initial internal gas pressure in the microbubble (= $[C_A + C_G]$ R T; where C_A and C_G = concentration of the filling air and gas respectively and T = absolute temperature); R_0 = initial microbubble radius; Γ = polytropic exponent of the gas; p_v = vapour pressure; p_o = ambient hydrostatic pressure; S_T = surface tension; $\delta_{\tau\sigma}$ = total damping constant (Church 1995); ω = angular frequency of the applied acoustic field; ρ = density of the surrounding medium; $P_{(t)}$ = time-varying applied acoustic pressure; η = shear viscosity of liquid; ω = driving frequency; t = time.

These differential equations predict that the surface shell supports a strain that counters the surface tension and thereby stabilizes the microbubble against dissolution.

2.3.3 Scattering Cross Section – Echogenicity of Microbubbles

The scattering cross-section, σ, is used as the parameter defining the acoustical behaviour of the microbubble and is defined as the quotient of the acoustic power scattered in all directions per unit incident

acoustic intensity. The scattered US intensity (I_s) is a function of the incident intensity I_0, the distance between the receiving transducer and the scatterer z, and the scattering cross-section of the scatterer σ according to:

$$I_s = \frac{I_0 \sigma}{4\pi z^2} \quad (21)$$

The scattering cross-section is directly related to the scattered acoustic power and to microbubble radius (Fig. 2.7) and inversely related to the applied pressure.

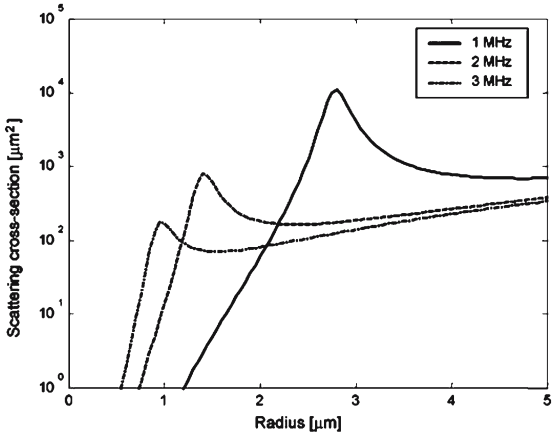

Fig. 2.7. Scattering cross section related to microbubble diameter for an encapsulated air-filled microbubble according to different frequencies of insonation. (Image courtesy of Peter JA Frinking, Bracco Research, Geneva, Switzerland)

The general expression for the scattering cross section in the frequency domain including higher harmonics is:

$$\sigma(R, \omega) = 4\pi R_0^{\,2} \frac{\Omega^4}{(1-\Omega)^2 + (\Omega\delta)^2} \quad (22)$$

where R = microbubble radius, R_0 = initial microbubble radius, ω = insonating frequency, $\Omega = \omega/f_0$ with f_0 = resonance frequency, δ = damping constant.

Equation 22, may be further developed as:

$$\sigma = \frac{4\pi R_0^{\,2}}{\left[\left(\frac{f_0}{f}\right)^2 - 1\right]^2} + \left(\frac{f_0}{f}\right)^4 \delta^2 \quad (23)$$

$$\sigma = \frac{4\pi}{9} k^4 R^6 \left[\left(\frac{k_s - k}{k}\right)^2 + \frac{1}{3}\left(\frac{3(\rho_s - \rho)}{2\rho_s + \rho}\right)^2\right] \quad (24)$$

where δ =damping constant, ρ =density respectively of the scatterer (subscript s, microbubble) and the surrounding medium (tissue or plasma), and k = adiabatic compressibility. The k and ρ are also related to the speed of sound ($c = 1/\sqrt{\rho k}$). Consequently, the scattering cross section is strongly dependent from frequency both for free air (Fig. 2.8) and encapsulated microbubbles (Fig. 2.9) and from the difference in density between the microbubble and the surrounding medium.

2.3.3.1 Practical Applications

At the resonant frequency, the scattering cross section of a microbubble is no longer simply dependent on its size, and can reach peak (Fig. 2.8, 2.9) values a thousand times higher compared to values at off-resonance frequencies (de Jong et al. 1996). Since the scattering cross section is strongly dependent on the ratio between the insonating frequency and the resonant frequency (Eq. 23), at frequency below resonance most of the scattering occurs at 180° relative to the incident wave, with an angular distribution pattern depending on the scatterer shape and the contrast in the acoustic properties between the particle and the surrounding medium (Coussios et al. 2004).

The compressibility (k value, see Eq. 24) of air is 7.65×10^{-6} m^2/N and the compressibility of water is 4.5×10^{-11} m^2/N, similarly to tissue and plasma, while

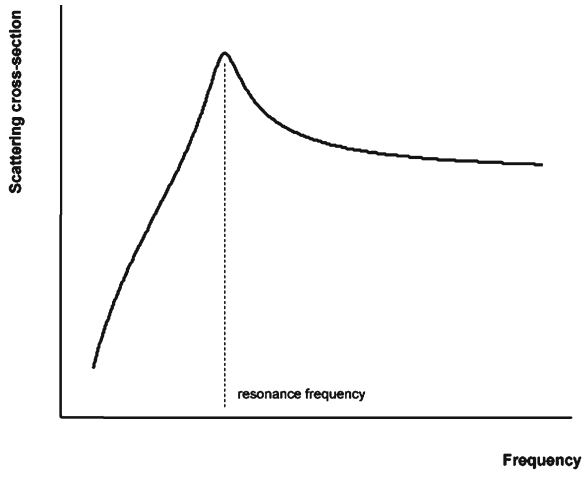

Fig. 2.8. Scattering cross section related to the insonating frequency for free-air microbubble. Scattering cross section abruptly increases at the resonance frequency of the microbubble. (Image courtesy of Peter JA Frinking, Bracco Research, Geneva, Switzerland)

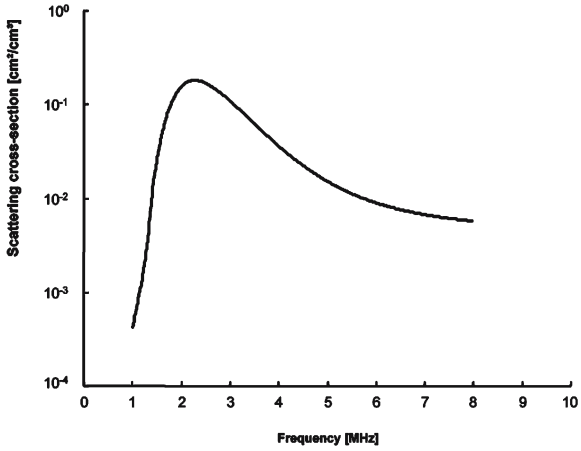

Fig. 2.9. Scattering cross section related to the insonating frequency for encapsulated air-filled microbubble. The lower the shell elasticity due to encapsulation, the higher the resonant frequency and the lower the scattering cross section and generation of harmonics. (Image courtesy of Peter JA Frinking, Bracco Research, Geneva, Switzerland)

the compressibility of a coated microbubble-based agent falls within this range (5×10^{-7} m^2/N in the case of Albunex). This high difference in compressibility, and so in impedance, results in a very high echogenicity which increases the sensitivity of US equipment to microbubbles (Dayton and Ferrara 2002).

Scattering cross-section equations may be simplified to:

$$\sigma = R_0{}^6 f_0{}^4 [\approx Z] \tag{25}$$

known as Born approximation, where R_0 is the initial microbubble radius, f_0 is the resonance frequency and Z is the difference in acoustic impedance (ratio of acoustic pressure to sound flow) between the surrounding medium and the microbubble. Encapsulation drastically reduces the influence of resonance frequency on scattering cross section since the lower the shell elasticity due to encapsulation, the higher the resonant frequency (Chatterjee and Sarkar 2003). Moreover, since Eq. 22 shows that the scattering cross section is inversely related to the damping constant, the encapsulation of microbubbles with a thick and stiff shell produces a lower scattering cross section also for the viscoelastic properties of the surrounding shell.

2.3.4 US Beam Attenuation and Microbubble Size Distribution

The US weakening results from *scattering* and *absorption*. The combined effect of scattering and attenuation depend on microbubble concentration (Fig. 2.10). Scattering is the prevalent phenomenon with low microbubble concentrations while the attenuation, caused by multiple scattering, dominates when the microbubble concentration increases.

$$a_{(f)} = \int_{R\,min}^{R\,max} n(r)\sigma(r)\,dr \tag{26}$$

where a(f) = US frequency-dependent attenuation coefficient expressed in nepers[Np]/length and nepers is a dimensionless quantity, R_{max} and R_{min} = minimum and maximum microbubble radii, n(r) = microbubble concentration and σ = scattering cross-section.

Equation 26 may be employed to calculate the microbubble size distribution which is in agreement

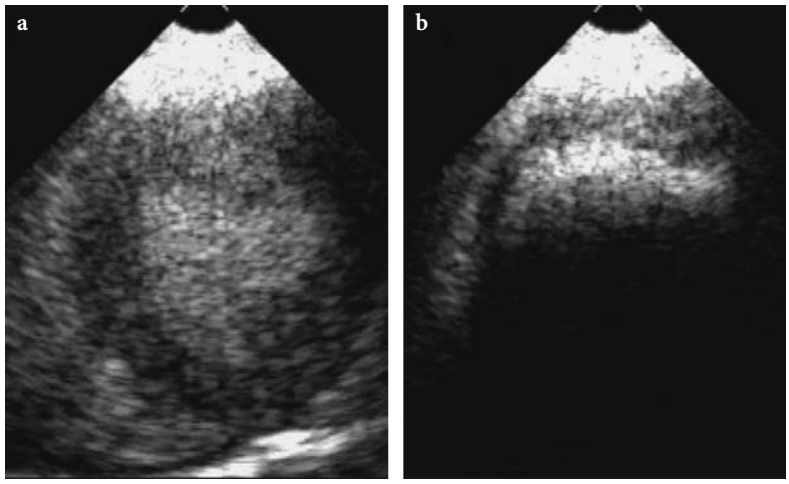

Fig. 2.10a,b. US attenuation determined by a microbubble-based agent (**a**). The attenuation expressed by the posterior acoustic shadowing increases by increasing microbubble concentration (**b**). (Images courtesy of Peter JA Frinking, Bracco Research, Geneva, Switzerland)

with values measured with optical methods. Microbubble-based agents size distribution is normal-shaped (Fig. 2.11) and the standard deviation is larger for first generation agents and lower for new generation agents which present a more uniform microbubble diameter.

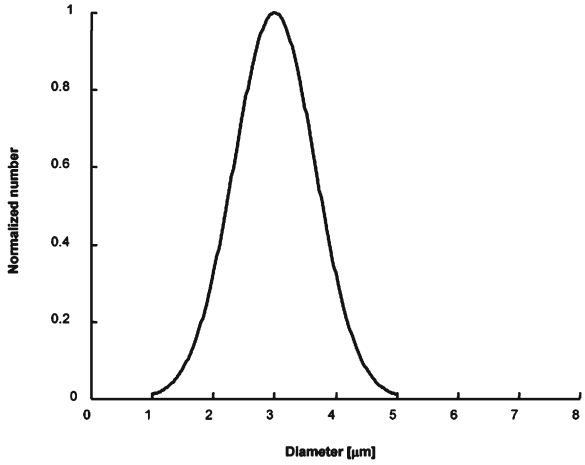

Fig. 2.11. Microbubbles diameter normal distribution. The mean diameter is 3 μm (Courtesy of Peter JA Frinking, Bracco Research, Geneva, Switzerland)

2.3.5 Scattering to Attenuation Ratio

In a suspension of microbubbles each microbubble has to be considered as an element which absorbs and scatters US at the same time. The total energy loss or attenuation for an acoustical beam travelling through a screen of microbubbles is called the extinction coefficient, $\mu_e(\omega)$, and is given by:

$$\mu_e(\omega) = \mu_a(\omega) + \mu_s(\omega) \tag{27}$$

where $\mu_a(\omega)$ is the absorption coefficient and $\mu_s(\omega)$ is the scattering coefficient.

The scattering to attenuation ratio (STAR) is a measure of the acoustical effectiveness of the contrast agent. The STAR is defined as:

$$\mathrm{STAR}(\omega) = \frac{\mu_s(\omega)}{\mu_e(\omega)} \tag{28}$$

and substituting Eq. 28 into Eq. 27 gives:

$$\mathrm{STAR}(\omega) = \frac{\mu_s(\omega)}{\mu_a(\omega) + \mu_s(\omega)} \tag{29}$$

where $\mu_s(\omega)$ represents the part of the energy that is scattered away omnidirectionally by the microbubbles, while $\mu_a(\omega)$ represents the part of the energy that is absorbed by the microbubbles.

Therefore, the lower the absorption of the incoming plane US wave, the higher the STAR. A maximum value of STAR = 1 is obtained when there is no absorption. However, this index is only valid for low acoustic pressures and at high acoustic pressures non-linear transient effects appear.

2.3.5.1 Practical Application

The attenuation of the acoustical beam travelling through a screen of microbubbles can cause shadowing of underlying biological structures and is not considered to be a useful parameter. An effective contrast agent, therefore, is defined by good scattering properties and low attenuation. For these reasons, the higher the STAR, the more effective the contrast agent. De Jong and Hoff (1993) and de Jong et al. (1994) showed a non-linear relation between the increase in the acoustic pressure of insonation and the produced backscattering and attenuation. Some experimental evidence (Coussios et al. 2004) suggests that liposomes present a higher scattering to attenuation ratio than albumin-coated microbubbles and could be more efficient as contrast agents.

2.3.6 Acoustic Power of Insonation

The probability for a single US pulse to destroy a microbubble (Fig. 2.12) increases for high acoustic power amplitudes, long US pulse lengths and low frequencies according to the following equation:

$$E_{\mathrm{acoustic}} = \int_o^k \left(P_0 \sin 2\pi f t\right)^2 dt = K P_0^{\,2} \frac{1}{f} \approx K(MI)^2 \tag{30}$$

where E_{acoustic} = acoustic power of insonation (W_0), P_0 = acoustic pressure amplitude, f = frequency, t = time, K = number of cycles per burst which determines the US pulse length, MI = mechanical index.

The acoustic power of insonation is usually considered related to the employed MI which measures the potential for mechanical damage to tissues exposed to intense US pulses.

$$MI = \frac{P -}{\sqrt{f}} \tag{31}$$

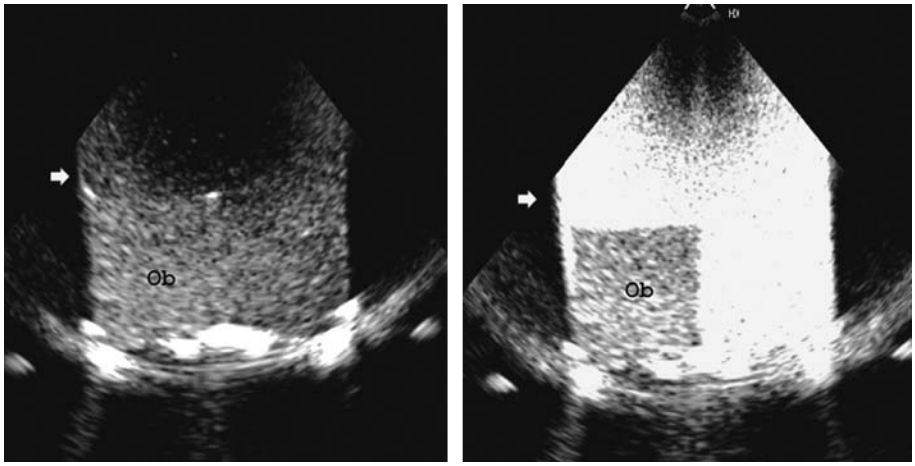

a b

Fig. 2.12a,b. Microbubble rupture shown in a tissue-simulating model. Microbubbles are suspended in a water bath containing a reference echoic object similar to tissues (*Ob*). At low acoustic power insonation (**a**) there is evidence of microbubble resonance with production of low intensity echoes (*arrow*). At high acoustic power insonation (**b**) there is evidence of microbubble destruction. The flash is produced by microbubble destruction (*arrow*) which produces a broadband frequency signal (Courtesy of Peter JA Frinking, Bracco Research, Geneva, Switzerland)

with the peak negative acoustic pressure (P–) in megapascals (MPa; 1 Pa = 1 Newton/m^2), and the frequency in MHz. In clinical practice, the range for MI varies from 0.05 to 1.9. The lower the frequency of US, the greater its MI and therefore its destructive properties. However, the MI is an unreliable predictor of microbubble destruction, since at the same MI value different values of acoustic powers of insonation may be measured in different US systems (Merritt et al. 2000).

2.3.6.1 High Acoustic Power

High acoustic power (Wo = peak negative pressure; 0.8–2.5 MPa) of insonation alters stabilized microbubbles and increases both the likelihood and rate of microbubble destruction (Shi et al. 2000). High acoustic power insonation induces changes of microbubble-based agents corresponding to fragmentation, coalescence, sonic cracking, jetting and to destruction of microbubbles (Dayton et al. 1999; de Jong et al. 1999; Postema et al. 2004).

Fragmentation is the fission of a bubble into smaller microbubbles (Postema et al. 2002, 2004) which was first visualized with high-speed cameras (Postema et al. 2001, 2004). Fragmentation occurs around peak microbubble contraction (Chomas et al. 2001), when the bubble collapse is driven by inertial forces because the inward acceleration continues to increase as the bubble approaches its minimus radius, and suddenly changes sign as the bubble begins a rebound (Postema et al. 2004). Coalescence is the fusion of two or more microbubbles. As adjacent microbubbles expand, the pressure in the film between them increases, resulting in a deformation of the bubble surfaces. This thinning continues until a critical thickness around 0.1 μm, at which Van der Waals attractive forces results in capsule rupture and the coalescence of the bubbles (Postema et al. 2004). Sonic cracking is the US-induced formation of a shell defect causing gas to escape from microbubbles (Postema et al. 2004), and it was observed with rigid-shell microbubbles (Postema et al. 2002). Jetting corresponds to asymmetric microbubble collapse, which causes the velocity of the upper bubble wall to exceed the velocity of the lower wall. For this phenomenon the fluid above the bubble is accelerated and focused during collapse, leading to the formation of a high-speed liquid jet (Postema et al. 2004).

US energy-mediated destruction, expressed as disappearance time, of microbubbles is directly related to US intensity, duration and frequency (Walker et al. 1997). Microbubble destruction produces the emission of a broadband frequency (Fig. 2.12) that includes both sub- and higher harmonics. The resulting fragments differ in their echo spectra and may be differentiated from the original microbubble-based contrast agent and subtraction contrast-specific modes, processing the echoes obtained before and after microbubble destruction (Dayton and Ferrara 2002), improve microbubble detection.

When the applied acoustic power exceeds a specific threshold, the scattering level increases abruptly for a few seconds producing an increased echogenic-

ity in conventional US and a coloured mosaic map at colour Doppler (Frinking 1999). The effect is most effective when the US wave hits the microbubble for the first time. This particular transient response, known also as stimulated acoustic emission or flash echo imaging, may be considered as a signature of each contrast agent and was particularly observed in some contrast agents such as Sonavist (Schering AG, Germany) and Quantison (Quadrant, UK).

2.3.6.2 Low Acoustic Power

Low acoustic power (Wo = peak negative pressure 100–600 kPa) is used to produce the non-linear harmonic response of microbubbles. Below an acoustic power threshold, microbubbles act as stable linear or non-linear scatterers depending on the applied acoustic power. With non-linear oscillation, the duration and degree of microbubble expansion is greater than its compression phase. Non-linear oscillations of microbubble-based contrast agents generate significant scattered echoes at harmonic multiples of the transmitted frequency (Fig. 2.12). These harmonic echoes may be differentiated from tissue echoes from their spectral characteristic, containing prevalently echoes at double frequency, from the lower acoustic power and from their phase. The more recently introduced contrast-specific modes employ pulse trains with multiple frequencies, amplitudes and phases which increase significantly the sensitivity to the harmonic signal produced by microbubbles (Chap. 4).

2.4 Artefacts from Microbubble-Based Agents

2.4.1 Microbubble Artefacts with Doppler

Most microbubble-specific artefacts are found with colour and power Doppler modes because the settings of US equipment become inappropriate following a strong increase of the backscattered signals (Fig. 2.13) and need to be recognized to avoid interpretative errors (Forsberg et al. 1994).

2.4.1.1 High-Intensity Transient Signals

This artefact is determined by microbubble collapse or by aggregates of macrobubbles producing sharp spikes on the Doppler spectral tracing, heard as crackling on the audio output (Figs. 2.14, 2.15). These spikes are easily recognized since they cover the entire frequency spectrum. This artefact may also be detected with colour and power Doppler imaging appearing as colour pixels of higher intensity within the more uniform signal of the vessel.

2.4.1.2 Pseudoacceleration of the Systolic Peak Velocity

An increase in the systolic peak velocity of up to 50% can be found at peak enhancement. This artefact is probably the result of signals that were too weak to be detected before microbubble injection and it may be almost completely cancelled by reducing the Doppler gain or by employing slow infusion of microbubbles. The increase in systolic peak velocity may produce error in grading stenotic lesions of the vessels.

2.4.1.3 Clutter

Clutter may be defined as unwanted strong echoes produced by stationary or slow moving tissues. The flow signals, registered at Doppler, are disturbed by clutter signals produced by muscular tissue and vessel walls which can be much stronger than the blood signals even after the injection of a microbubble-based contrast agent. These signals are also produced by the relative movement

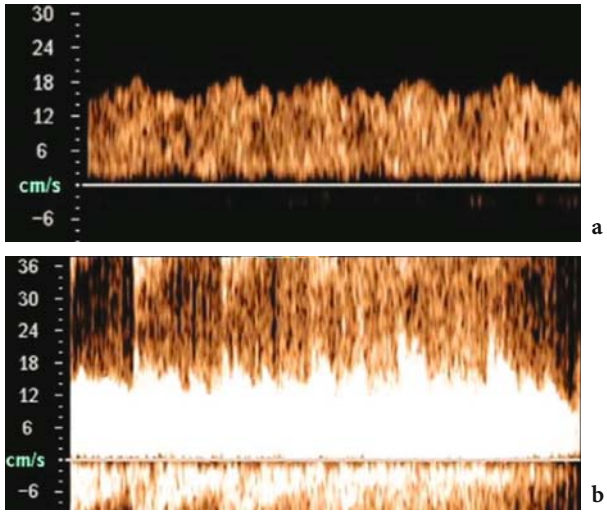

Fig. 2.13a,b. Artefacts from microbubble-based agents. Doppler signal before microbubble injection (**a**). Excessive amplifications of Doppler signal after microbubble injection (**b**)

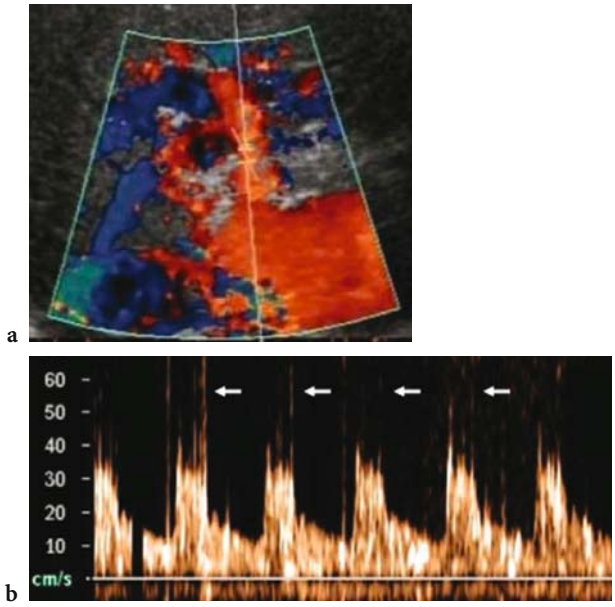

Fig. 2.14a,b. Artefacts from microbubble-based agents. Spikes (*arrows*) due to macrobubble presence in the bloodstream. Colour Doppler and Doppler interrogation of the hepatic artery (**a**) after microbubble injection. In the Doppler spectra (**b**) different spikes, covering the entire frequency spectrum, are evident due to macrobubble aggregates

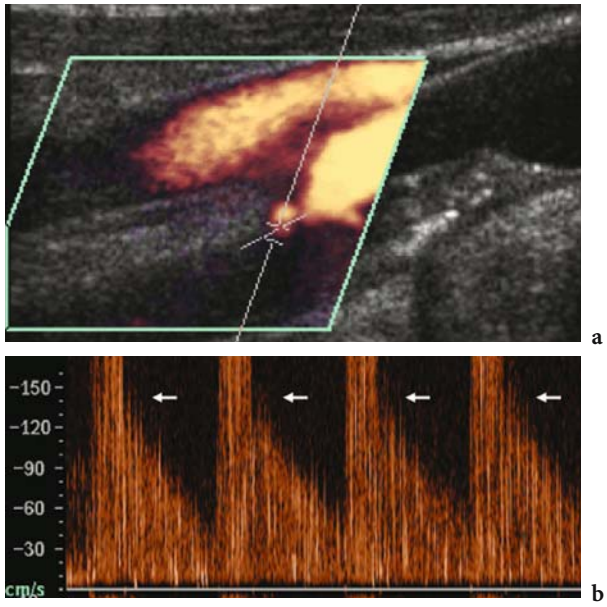

Fig. 2.15a,b. Artefacts from microbubble-based agents. Spikes (*arrows*) due to macrobubble presence in the bloodstream. Colour Doppler and Doppler interrogation of the internal carotid artery (**a**) after microbubble injection. In the Doppler spectra (**b**) different spikes are evident due to macrobubble aggregates or microbubbles collapse

between the US probe and the unwanted tissue targets due to the cardiac beating, patient breathing and the operator moving while keeping the probe. Clutter may be reduced by using specific filters, harmonic power Doppler (Chap. 4) or by contrast-specific modes as three stage multi-pulse contrast agent detection (Frinking et al. 1998; Kirkhorn et al. 2001). The principle of this multi-pulse technique is that the scattering properties are modified if microbubbles are insonated at high acoustic power while remaining unchanged at low acoustic power. The first stage of the pulsing sequence is to use low acoustic power pulses to obtain high resolution reference images without altering the agents; the second stage is to use high acoustic power, called the release burst, to modify the agent; and the third stage is to detect the changes using low acoustic power.

2.4.1.4 Blooming Artefact

In Doppler tracing only the mean frequency shift is displayed, while the Doppler signal intensity is increased after microbubble injection since the increase in backscattering echo-signal intensity determines the appearance also of the lowest velocities that were too weak to be registered before microbubble injection. When colour or power Doppler is turned on the overload of the Doppler signal registration apparatus is determined by the strong signals and multiple re-reflections between adjacent microbubbles. Such artefact (Figs. 2.16, 2.17) can be limited by reducing the colour gain and persistence and the MI or by increasing the wall filter and the pulse repetition frequency, resulting in a decreased sensitivity of the system. The slow infusion of microbubbles limits this artefact because of a decrease in the peak signal intensity. Dedicated US contrast-specific modes were introduced principally to avoid this artefact.

2.4.1.5 Jail Bar Artefact

The jail bar artefact (Fig. 2.18) is prevalently observed with power Doppler mode. It is determined by an error in image interpolation when the management of the backscattering signal intensity from the US system approaches saturation. Since each frame is reconstructed from an interpolation mathematical procedure of the image view lines, the saturation of signal determines a lack of colour along the interpolating view.

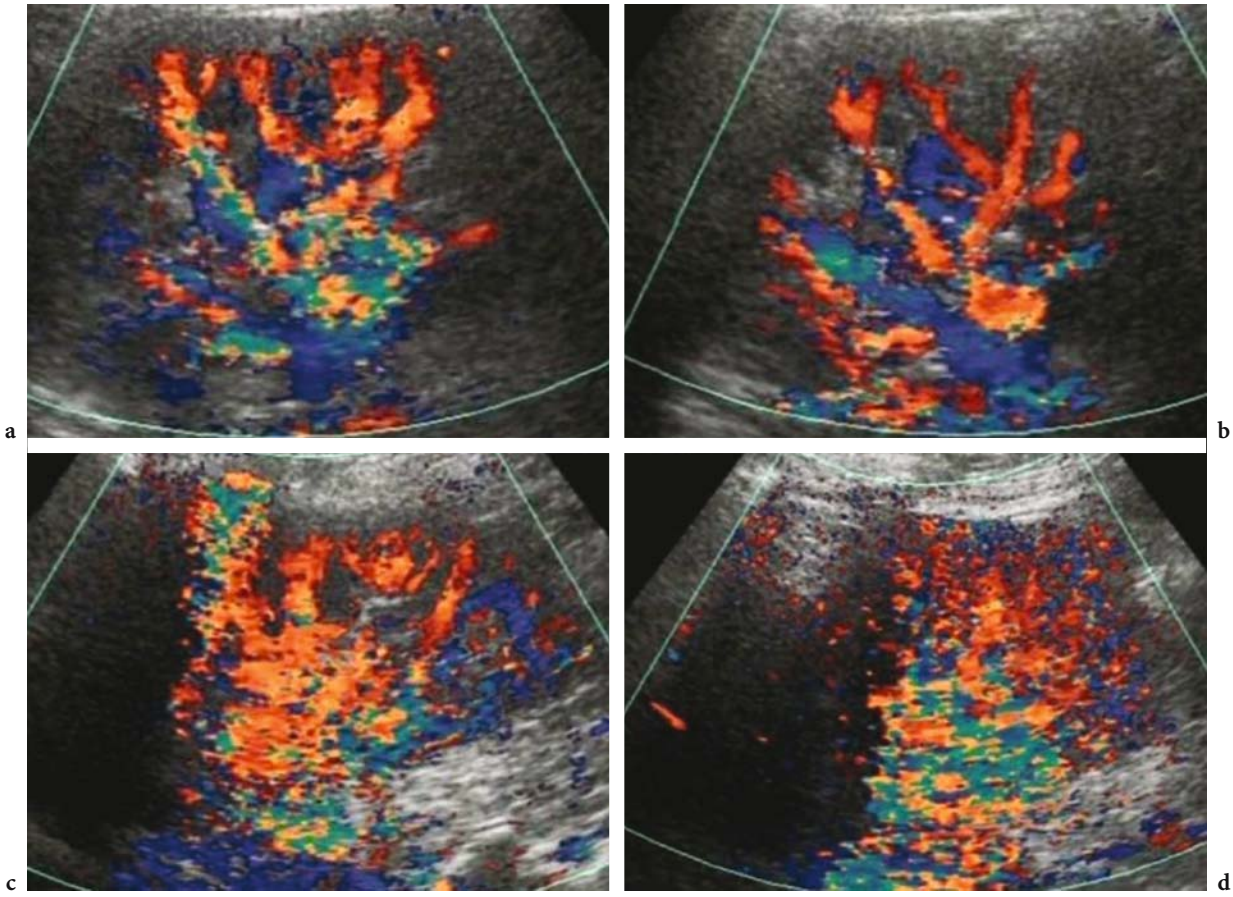

Fig. 2.16a–d. Artefacts from microbubble-based agents. Blooming artefact consisting in the presence of colour signal outside the vessels. Baseline colour Doppler US (**a,b**) of the right kidney. The renal parenchymal vessels are identified. After microbubble-based agents injection (**c,d**) colour signal becomes diffuse and identified outside the renal vessels

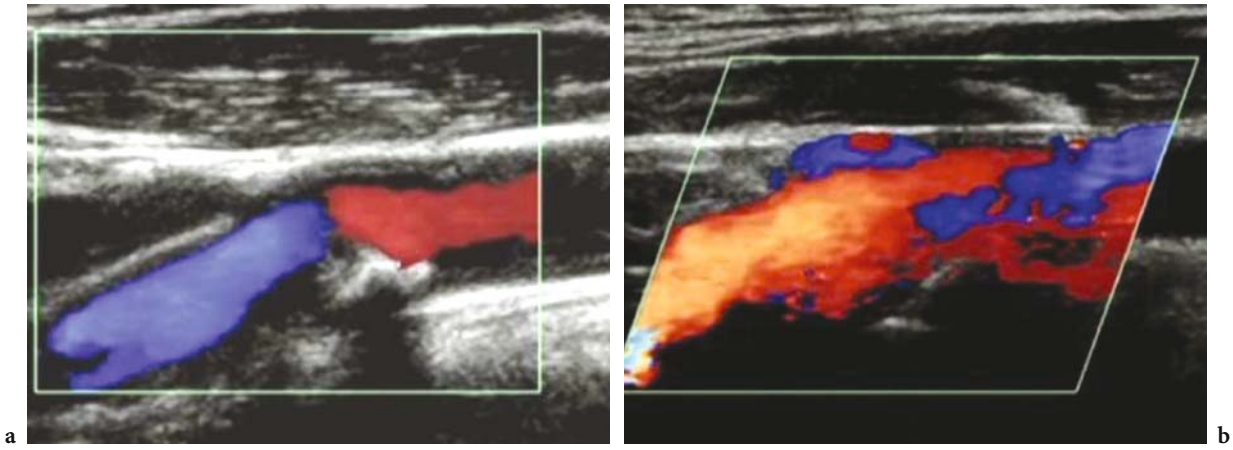

Fig. 2.17a,b. Artefacts from microbubble-based agents. Blooming artefact consisting in the presence of colour signal outside the vessels. Baseline colour Doppler US (**a**) of the right carotid bulb. After microbubble-based agents injection (**b**) colour signal becomes diffuse and identified outside the carotids

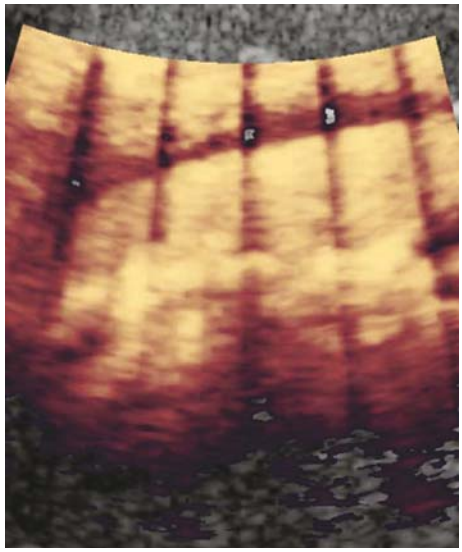

Fig. 2.18. Artefacts from microbubble-based agents. Jail-bar artefact consisting in the presence of black vertical signals void throughout the image

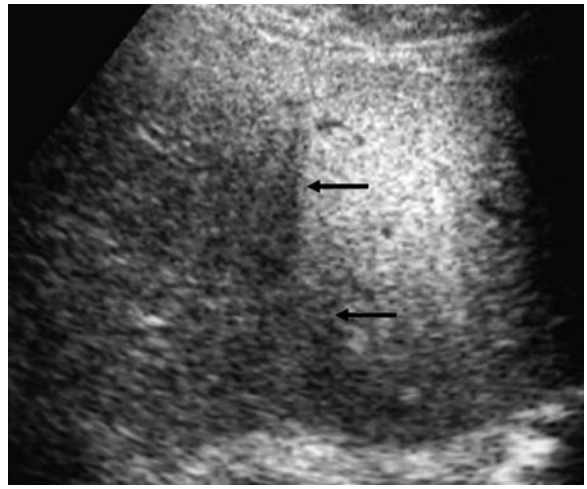

Fig. 2.19. Artefacts from microbubble-based agents (*arrows*). Artefact arising from the second scan in the same region of the liver. The areas of the liver where microbubbles were previously destroyed (*arrows*) appear as hypoechoic if compared to the adjacent areas of the liver not previously scanned

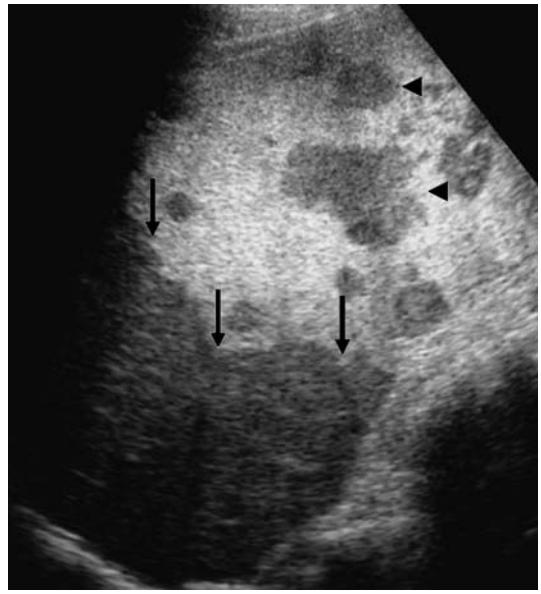

Fig. 2.20. Microbubble artefacts. Artefact (*arrows*) arising from the second scan in the same region of the liver. The areas of the liver where microbubbles were previously destroyed appear as hypoechoic compared to the adjacent areas of the liver not previously scanned. Some liver metastases are also evident (*arrowheads*)

2.4.2 Microbubble Artefacts with Contrast-Specific Modes

2.4.2.1 Attenuation of the Sound Beam

This artefact is produced when the sound beam travels through high concentrations of microbubble-based agents (Jakobsen and Correas 2001). This artefact is frequently observed in the heart, and sometimes also observed in the liver.

2.4.2.2 Artefact from Multiple Insonations

This artefact results from different scans performed orthogonally which causes microbubble disruption, e.g. when the right liver lobe is scanned at a transverse insonating plane after initial longitudinal sweep through the left lobe and part of the right lobe (Figs. 2.19, 2.20) (Harvey et al. 2000). Another artefact consisting in vertical signal void may be determined by small tissue movement between the two out-of-phase pulses in pulse inversion mode (Fig. 2.21) and may be eliminated by power pulse inversion mode which works as a multi-pulse technique by considering as linear the tissue movement between the different pulses and by summing the resulting phase shift.

2.4.2.3 Artefact from Heterogeneous Rate of Microbubble Rupture

Destructive mode presents some technical disadvantages. To produce a uniform microbubble rup-

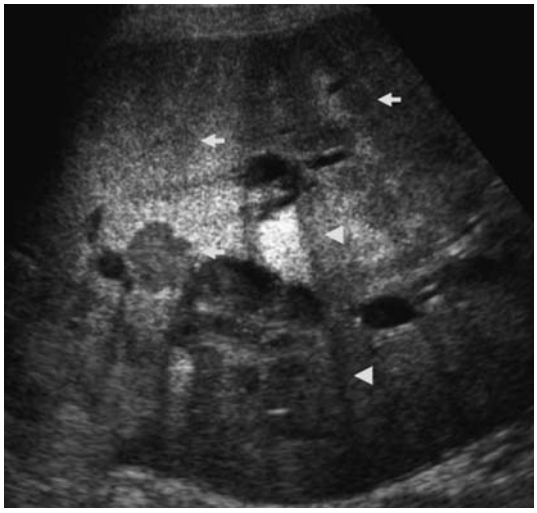

Fig. 2.21. Artefacts from microbubble-based agents. Pulse inversion mode. Artefacts arising from stationary tissue movement (*arrowheads*) between the first and the second out-of-phase pulse which determines the cancellation of the signal. Liver metastases (*arrows*) are also identified

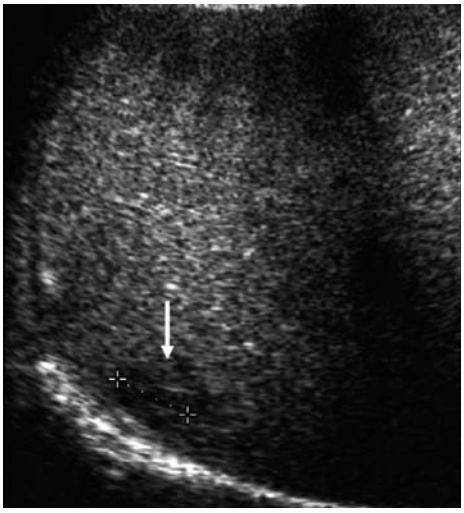

Fig. 2.22. Artefacts from microbubble-based agents. Pulse inversion mode. Artefact arising from heterogeneous microbubble rupture throughout the liver parenchyma which simulate one focal liver lesion (*arrow*) adjacent to the diaphragm

ture on liver parenchyma, which is necessary to produce a wideband frequency signal, rapid and uniform sweeps are necessary. The largest amount of microbubbles entrapped in liver sinusoids are destroyed after one single high MI sweep, so there is no possibility to analyze focal liver lesions with US acoustic windows other than transabdominal, such as an intercostal view. Scanning irregularities determined by a not completely uniform sweep or liver movements during emission of the two out phase pulses or to the heterogeneous distribution of acoustic power produce artefacts simulating focal liver lesions (Fig. 2.22). In order to reduce bubble destruction and to prolong bubble permanence, the lowest real time frame rate (7–9 Hz) has to be employed. However, a low frame rate increases US artefacts related to motion and to bubble rupture heterogeneously, which can simulate focal liver defects producing focal positive findings misinterpreted as metastases.

References

Anderson AL, Hampton LD (1980) Acoustics of gas-bearing sediments. Background. J Acoust Soc Am 67:1865-1889

Bauer A, Blomley MJK, Leen E, Cosgrove D, Schlief R (1999) Liver-specific imaging with SHU 563 A: diagnostic potential of a new class of ultrasound contrast media. Eur Radiol 9 [Suppl 3]:S349-S352

Chatterjee D, Sarkar K (2003) A Newtonian rheological model for the interface of microbubble contrast agents. Ultrasound Med Biol 29:1749-1757

Chomas JE, Dayton P, May D, Ferrara K (2001) Threshold of fragmentation for ultrasonic contrast. J Biomed Opt 6:141-150

Church CC (1995) The effect of an elastic solid surface layer on the radial pulsation of gas bubbles. J Acoust Soc Am 97:1510-1521

Correas JM, Kessler D, Worah D, Quay SC (1997) The first phase shift ultrasound contrast agent: EchoGen. In: Goldberg BB (ed) Ultrasound contrast agents. Dunitz, London, pp 83-99

Correas JM, Burns PN, Lai X, Qi X (2000) Infusion versus Bolus of an ultrasound contrast agent: in vivo dose-response measurements of BR1. Invest Radiol 35:72-79

Correas JM, Bridal L, Lesavre A et al (2001) Ultrasound contrast agents: properties, principles of action, tolerance, and artifacts. Eur Radiol 11:1316-1328

Coussios CC, Holland CK, Jakubowska L et al (2004) In vitro characterization of liposomes and Optison by acoustic scattering at 3.5 MHz. Ultrasound Med Biol 30:181-190

Dayton PA, Ferrara KW (2002) Targeted imaging using ultrasound. J Magn Res Imaging 16:362-377

De Jong N, Hoff L (1993) Ultrasound scattering properties of Albunex® microspheres. Ultrasonics 31:175-181

De Jong N, Hoff L, Skotland T, Bom N (1992) Absorption and scatter of encapsulated gas filled microspheres: theoretical considerations and some measurements. Ultrasonics 30:95-103

De Jong N, Cornet R, Lancée CT (1994a) Higher harmonics of vibrating gas filled microbubbles, part one: simulations. Ultrasonics 32:447-453

De Jong N, Cornet R, Lancée CT (1994b) Higher harmonics of vibrating gas filled microbubbles, part two: measurements. Ultrasonics 32:455-459

De Jong N, Frinking P, ten Cate F, van der Wouw P (1996) Characteristics of contrast agents and 2D imaging. IEEE ultrasonics symposium, pp 1449-1458

De Jong N, Frinking PJ, Bouakaz A et al (1999) Optical imaging of contrast agent microbubbles in an ultrasound field with a 100-MHz camera. Ultrasound Med Biol 26:487-492

Fisher NG, Christiansen JP, Leong-Poi H et al (2002) Myocardial and microcirculatory kinetics of BR14, a novel third-generation intravenous ultrasound contrast agent. J Am Coll Cardiol 39:530-537

Forsberg F, Tao Shi W (2001) Physics of contrast microbubbles. In: Goldberg B, Raichlen JS, Forsberg F (eds) Ultrasound contrast agents: basic principles and clinical applications. Dunitz, London, pp 15-23

Forsberg F, Basude R, Liu JB et al (1999) Effect of filling gasses on the backscatterer from contrast microbubble: theory and in vivo measurements. Ultrasound Med Biol 25:1203-1211

Frinking PJA, Céspedes EI, de Jong N (1998) Multi-pulse ultrasound contrast imaging based on a decorrelation detection strategy. Proc IEEE Ultras Symp 2:1787-1790

Frinking PJA (1999) Ultrasound contrast agents: acoustic characterization and diagnostic imaging. Optima Grafische Communicatie, Rotterdam, pp 33-37

Frinking PJA, de Jong N (1999) Scattering properties of encapsulated gas bubbles at high ultrasound pressures. J Acoust Soc Am 105:1989-1996

Forsberg F, Goldberg BB, Liu JB (1996) On the feasibility of real time in vivo harmonic imaging with proteinaceous microspheres. J Ultrasound Med 15:853-860

Gorce JM, Arditi M, Schneider M (2000) Influence of bubble size distribution on the echogenicity of ultrasound contrast agents: a study of SonoVue. Invest Radiol 35:661-671

Gramiak R, Shah PM (1968) Echocardiography of the aortic root. Invest Radiol 3:356-366

Harvey CJ, Blomley MJ, Eckersley RJ et al (2000) Hepatic malignancies: improved detection with pulse inversion US in late phase of enhancement with SH U 508 A - early experience. Radiology 216:903-908

Harvey CJ, Blomley MJK, Eckersley RJ, Cosgrove DO (2001) Developments in ultrasound contrast media. Eur Radiol 11:675-689

Hauff P, Fritsch T, Reinhardt M et al (1997) Delineation of experimental liver tumors in rabbits by a new ultrasound contrast agent and stimulated acoustic emission. Invest Radiol 32:94-99

Hoff L (1996) Acoustic properties of ultrasonic contrast agents. Ultrasonics 34:591-593

Jakobsen JA, Correas JM (2001) Ultrasound contrast agents and their use in urogenital radiology: status and prospects. Eur Radiol 11:2082-2091

Kabalnov A, Klein D, Pelura T et al (1998a) Dissolution of multicomponent microbubble in the blood stream 1. Theory. Ultrasound Med Biol 24:739-749

Kabalnov A, Bradley JA, Flam S et al (1998b) Dissolution of multicomponent microbubble in the blood stream 2. Experiment. Ultrasound Med Biol 24:751-760

Kono Y, Steinbach GC, Peterson T et al (2002) Mechanism of parenchymal enhancement of the liver with a microbubble-based US contrast medium: an intravital microscopy study in rats. Radiology 224:253-257

Lindner JR, Dayton PA, Coggins MP et al (2000) Noninvasive imaging of inflammation by ultrasound detection of phagocytosed microbubbles. Circulation 102:531-538

Marelli C (1999) Preliminary experience with NC100100, a new ultrasound contrast agent for intravenous injection. Eur Radiol 9 [Suppl 3]:S343-S346

Medwin H (1977) Counting bubbles acoustically: a review. Ultrasonics 1:7-13

Merritt CR, Forsberg F, Shi WT et al (2000) The mechanical index: an inappropriate and misleading indicator for desctruction of ultrasound microbubble contrast agents. Radiology 217:395

Meuwl JY, Correas JM, Bleuzen A, Tranquart F (2003) Detection modes of ultrasound contrast agents. J Radiol 84:2013-2024

Morel DR, Schwieger I, Hohn L et al (2000) Human pharmacokinetics and safety evaluation of SonoVue™, a new contrast agent for ultrasound imaging. Invest Radiol 35:80-85

Powers JE, Burns PN, Souquet J (1997) Imaging instrumentation for ultrasound contrast agents. In: Nanda NCSR, Goldberg BB (eds) Advances in echo imaging using contrast enhancement. Kluwer, Dordrecht, pp 137-170

Postema M, Bouakaz A, Chin CT, de Jong N (2001) Real-time optical imaging of individual microbubbles in an ultrasonic field. Proc IEEE Ultras Symp 1679-1682

Postema M, Bouakaz A, Chin CT, de Jong N (2002) Optically observed microbubble coalescence and collapse. Proc IEEE Ultras Symp 1900-1903

Postema M, van Wamel A, Lancée CT, de Jong N (2004) Ultrasound-induced encapsulated microbubble phenomena. Ultrasound Med Biol 30:827-840

Quaia E, Blomley MJK, Patel S et al (2002) Initial observations on the effect of irradiation on the liver-specific uptake of Levovist. Eur J Radiol 41:192-199

Rayleigh (1917) On the pressure developed in a liquid during the collapse of a spherical cavity. Philos Mag 34:94-98

Schneider M, Arditi M, Barrau MB et al (1995) BR1: a new ultrasonographic contrast agent based on sulphur hexafluoride-filled microbubbles. Invest Radiol 30:451-457

Schneider M, Broillet A, Bussat P et al (1997) Gray-scale liver enhancement in VX2 tumor bearing rabbits using BR14, a new ultrasonographic contrast agent. Invest Radiol 32:410-417

Shankar PM, Krishna PD, Newhouse VL (1998) Advantages of subharmonic over second harmonic backscatterer for contrast-to-tissue echo enhancement. Ultrasound Med Biol 24:395-399

Shen CC, Li PC (2003) Pulse-inversion-based fundamental imaging for contrast detection. IEEE Trans Ultrason Ferroelectr Freq Control 50:1124-1133

Shi WT, Forsberg F, Tornes A et al (2000) Destruction of contrast microbubbles and the association with inertial cavitation. Ultrasound Med Biol 26:1009-1019

Takeuchi H, Ohmori K, Kondo I (2004) Interaction with leukocytes: phospholipid-stabilized versus albumin-shell microbubbles. Radiology 230:735-742

Walker KW, Pantely GA, Sahn DJ (1997) Ultrasound-mediated destruction of contrast agents. Effect of ultrasound intensity, exposure, and frequency. Invest Radiol 32:728-734